Electrochemical performance of Co_3O_4/CeO_2 electrodes in H_2S/H_2O atmospheres in a proton-conducting ceramic symmetrical cell with $BaZr_{0.7}Ce_{0.2}Y_{0.1}O_3$ solid electrolyte

Tz. Kraia[a,b,c], S. Wachowski[c,d], E. Vøllestad[c], R. Strandbakke[c], M. Konsolakis[e], T. Norby[c], G.E. Marnellos[a,b,f]

[a] Department of Mechanical Engineering, University of Western Macedonia, Kozani, Greece
[b] Chemical Process & Energy Resources Institute, CE.R.T.H., Thessaloniki, Greece
[c] University of Oslo, Department of Chemistry, Centre for Materials Science and Nanotechnology, Oslo, Norway
[d] Department of Solid State Physics, Faculty of Applied Physics and Mathematics, Gdansk University of Technology, Gdansk, Poland
[e] School of Production Engineering and Management, Technical University of Crete, Chania, Greece
[f] Department of Environmental Engineering, University of Western Macedonia, Kozani, Greece

ARTICLE INFO

Keywords:
H_2S-tolerant electrodes
Cobalt-ceria oxides
BZCY72

ABSTRACT

The electrochemical performance of Co_3O_4/CeO_2 mixed oxide materials as electrodes, when exposed to H_2S/H_2O atmospheres, was examined employing a proton conducting symmetrical cell, with $BaZr_{0.7}Ce_{0.2}Y_{0.1}O_3$ (BZCY72) as the solid electrolyte. The impact of temperature (700–850 °C) and H_2S concentration (0–1 v/v%) in steam-rich atmospheres (90 v/v% H_2O) on the overall cell performance was thoroughly assessed by means of electrochemical impedance spectroscopy (EIS) studies. The performance of the Co_3O_4/CeO_2 electrode was significantly enhanced by increasing the H_2S concentration and temperature. The obtained results were interpreted on the basis of EIS results and physicochemical characterization (XRD, SEM) studies of fresh and used electrodes. Notably, it was found that the mass transport processes, mainly associated with the adsorption and diffusion of the intermediate species resulting by the chemical and half-cell reactions taking place during cell operation, dominate the electrode polarization resistance compared with the charge transfer processes. Upon increasing temperature and H_2S concentration, the electrode resistance is substantially lowered, due to the in situ activation and morphological modifications of the electrode, induced by its interaction with the reactants (H_2S/H_2O) and products (H_2/SO_2) mixtures.

1. Introduction

Today, emerging energy and environmental concerns force society to utilize “clean” fuel resources and efficient conversion technologies [1]. Initiatives, like the global Paris Agreement [2], point to the need for a massive penetration of intermittent renewable power sources (IRES) to form the backbone for a sustainable future. However, in order to use that green power, efficient energy storage solutions such as the use of hydrogen, should be developed to power all needs and applications that society now takes for granted, from heating to transportation.

Hydrogen, if derived from carbon-free energy resources, is worldwide acknowledged as an environmental friendly energy vector, which can support future energy developments. Among the different sustainable approaches for hydrogen production, the decomposition of hydrogen sulfide (H_2S) using the excess electricity of IRES, is of particular interest. H_2S is present in various quantities in industrial waste streams, oil and natural gas reserves, geothermal and volcanic activity areas, oceans, and maritime deep waters [3]. In addition, H_2S that is abundantly found in Black Sea waters (produced by sulfur reducing bacteria), hails as a potential H_2 source, while its removal from the Black Sea waters will contribute to the sufficient environmental protection of the surrounding ecosystem [4].

The current industrial practice for H_2S management involves the well-known Claus process, a partial oxidation treatment, which allows the recovery of elemental sulfur (S_n) at the expense of hydrogen consumption to water. Several alternatives have been proposed for the production of hydrogen from H_2S decomposition, which are currently at different stages of development, involving thermochemical, photochemical, plasma-chemical and electrochemical methods [5,6]. The majority of these approaches present certain disadvantages attrib-

http://dx.doi.org/10.1016/j.ssi.2017.04.010

uted to the particular high energy requirements and low efficiencies, rendering their commercialization still in doubt.

Recently, researchers suggested an electrochemical approach at high temperatures to efficiently generate and separate, in a single step, pure H_2 from H_2S electrolysis, employing a proton conducting ceramic membrane reactor [7–10]. However, one of the major challenges is the optimal selection of cell materials and especially of the anode electrode, which will be exposed to a H_2S-containing reacting mixture and generate the protons to be transported through the H^+-conducting solid electrolyte to the cathode, where pure hydrogen is formed.

The anode material has to exhibit high electro-catalytic activity toward H_2S decomposition, high electronic/ionic conductivity, good adherence on the solid electrolyte surface, and tolerance to H_2S rich environments [11,12]. Several sulfides, oxides and metals have been investigated for this purpose, reviewed in [12]. Among the various sulfur resistant anode materials, thiospinels and metal sulfides are favorable for H_2S oxidation fuel cells, however their time-consuming and complex synthesis procedure along with their rather low electro-catalytic activity and insufficient chemical stability limit their applicability in real processes [11].

Ceria-based mixed oxides have recently gained considerable attention in the field of electro-catalysis due to their sufficient electrochemical performance and resistance to poisons. For instance, Co_3O_4/CeO_2 materials have been extensively applied in the field of solid oxide fuel cells (SOFCs), since they combine enhanced electronic conductivity and electro-catalytic activity [13,14]. Recently, the superior catalytic performance of Co_3O_4/CeO_2 composites toward H_2S decomposition to H_2 in both dry and wet (90 v/v%) atmospheres was also demonstrated [15].

In the present work, the electrochemical performance and stability of Co_3O_4/CeO_2 composite electrodes in H_2S atmospheres containing excess H_2O (90 v/v%) is examined in a single-chamber proton conducting ceramic symmetrical cell, employing $BaZr_{0.7}Ce_{0.2}Y_{0.1}O_3$ (BZCY72) as a proton conducting solid electrolyte material. AC impedance spectroscopy studies at different H_2S concentrations (0–1 v/v%) and temperatures (700–850 °C) accompanied by XRD and SEM physicochemical characterizations of the fresh and aged electrodes revealed the stable electrochemical performance of Co_3O_4/CeO_2 composites, opening new horizons for the efficient management of H_2S-containing streams toward IRES-powered electrochemical hydrogen production.

2. Materials and methods

2.1. Synthesis of composite oxides

Commercially available powders of Cobalt Oxide, Co_3O_4 (Sigma Aldrich), and Cerium Oxide, CeO_2 (Alfa Aesar), were used as the starting materials. Initially, the oxides were separately milled in isopropanol with the aid of a planetary ball mill using agate grinding balls and cups (4 h, at 300 rpm). The resulting powders were subsequently mixed in a weight ratio of 1:1, without any sintering agent, and milled in isopropanol for 40 min at 200 rpm, using zirconium balls and cups, to homogenize the composite mixture. The resulting slurry was finally left to dry at 100 °C overnight.

2.2. Cell preparation

BZCY72 (NorECs, Oslo, Norway) in the form of disk (ca. 2 cm diameter and 1 mm thickness), was employed as proton-conducting ceramic solid electrolyte, having less than 100 ppm Ni content and an estimated density of ca. 99% [16]. Prior to electrodes deposition, the BZCY72 disk was polished with SiC paper to obtain good adherence of the electrode on the electrolyte surface. In the following, two porous Co_3O_4/CeO_2 electrode films were deposited on both sides of the BZCY72 disk.

The Co_3O_4/CeO_2 oxides ink was prepared by mixing the dried composite oxide powders with a commercial (NexTech Materials) organic ink vehicle VEH at a 1:2 weight ratio, and stirred at 400 rpm overnight. The optimal thin film layers preparation procedure was achieved by applying the resulting viscous suspension in two steps. In the first step, one layer was printed symmetrically on both sides of the dense electrolyte, with the aid of a blade, and dried for 30 min at 100 °C. The same procedure was repeated for the second layer deposition step. Afterwards, the cell was heated at 1400 °C for 5 h in ambient air, followed by cooling to room temperature, at a constant rate of 1 °C/min. In addition, there was also an intermediate heating stage at 600 °C for 1 h, to remove polyvinyl butyral (PVB). The amount of the deposited films on both sides of the BZCY72 disk (difference between the weight of the dried solid electrolyte disk and the cell weight after electrodes deposition and calcination) was equal to 100–110 mg for each electrode, resulting in an apparent area equal to 0.25 cm^2. For cell completion, a fine-masked gold mesh was pressed down on the electrode to act as the current collector, while gold wires served as current leads.

2.3. Characterization studies

The morphological characterization of the electrodes, as well as the cross sectional features of the cell before and after electrochemical measurements was carried out by use of scanning electron microscopy, SEM (JEOL JSM 6300), supported with energy dispersive X-ray spectroscopy (EDS). The sample was attached to a metal sample holder, using carbon tape, and coated with a thin gold layer. The crystalline structure was determined using the X-ray powder diffraction (XRD) method. A Siemens D 500 diffractometer was employed for the XRD measurements with a Cu Kα radiation (λ = 0.154 nm) operated at 40 kV and 30 mA. Diffractograms were collected in the 2θ = 10°–80° range at a scanning rate of 0.04° over 2 s. The DIFFRAC plus Basic data evaluation software was employed to identify the diffraction peaks.

2.4. Experimental setup and reactor design

The gas flow experimental set-up to examine the electrochemical performance of the Co_3O_4-CeO_2/BZCY72/Co_3O_4-CeO_2 symmetrical cell was similar to that described in our previous work [4], and consisted of i) the gas feeding unit with the cylinders of the employed gas mixtures (pure Ar and H_2S/Ar) and the corresponding mass flow controllers, ii) the pump for liquid H_2O feed and the heater for H_2O vapors incorporation into the cell reactor, iii) the cell reactor, iv) a condenser located just after the cell reactor to remove the unreacted H_2O, v) a sulfur scrubber located before the gas analysis system to remove the S-containing chemical species, vi) the Gas Chromatograph to monitor the generated H_2 at the cell reactor effluent and vii) the electrochemical workstation connected to the cell.

A custom-made single chamber reactor cell testing system was employed, as shown in Fig. 1. It consists of a stainless steel head, which incorporates specific provisions for reactants feed and products removal, and to which a quartz tube (150 mm long, ID = 37 mm, OD = 40 mm) is accommodated. The quartz tube is equipped with a cooling ring (SS 316) and a Viton O-ring for sealing. The cell was located inside the quartz tube, and both electrodes were exposed to the same reaction atmosphere. Two thin Au wires contacting the electrodes were used to hold the cell suspended inside the quartz tube and to electrically connect the cell to the Versa Stat 4 electrochemical workstation. Quartz tubes (ID = 1 mm, OD = 3 mm) were employed to insulate the Au wires from the reactor head and Ultra Torr fittings held the tubes in place. The top of these tubes was sealed by placing and melting at open flame a small (about 1 cm long) piece of 1/8″ polyethylene tube.

In each reaction condition, the generated hydrogen at the effluent stream was recorded in an on-line Gas Chromatograph (Trace GC

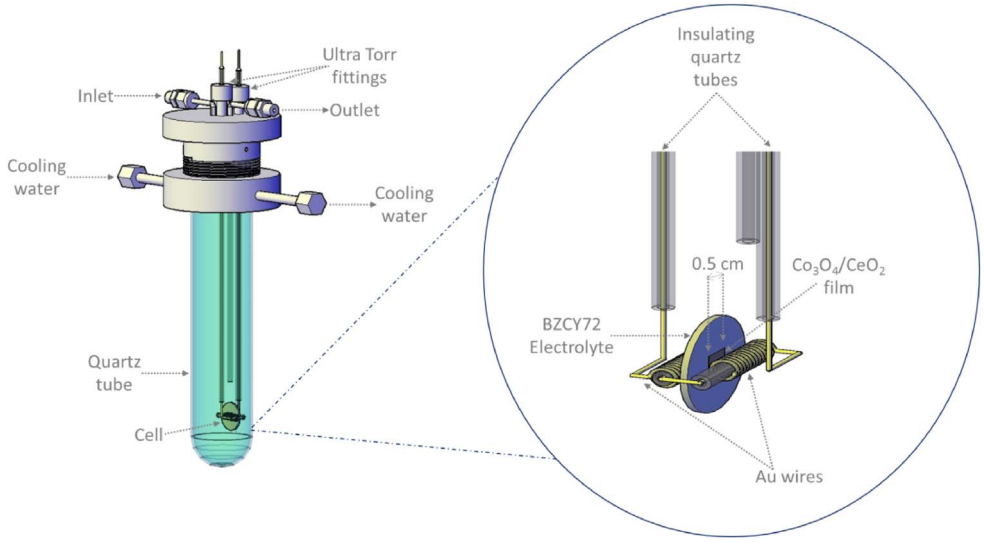

Fig. 1. Schematic representation of the single chamber symmetrical proton conducting cell, Co_3O_4-CeO_2/BZCY72/Co_3O_4-CeO_2.

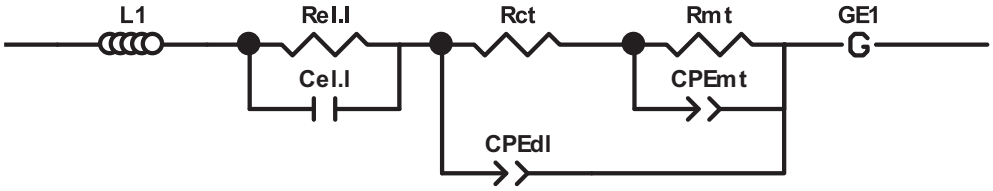

Fig. 2. Equivalent circuit model, representing electrolyte resistance (Rel.l) and capacitance (Cel.l), charge transfer resistance (Rct) and double layer pseudo-capacitance (CPEdl), mass transfer resistance (Rmt) and pseudo-capacitance (CPEmt), and Gerischer impedance (G).

Ultra), equipped with a thermal conductivity detector, and a Molecular Sieve 5A column.

2.5. Electrochemical impedance spectroscopy (EIS) studies

All EIS experiments were conducted under atmospheric pressure, at temperatures between 700 and 850 °C and the total flow rate of the reacting mixture equaled to 100 cm^3/min. Prior to experiments, inert argon (99.999% purity, Air Liquide), with a flowrate of 100 cm^3/min, was introduced into the cell reactor, while the temperature was steadily increased up to the set point temperature, with a heating rate of 3 °C/min. When the selected temperature was reached, water vapor (90 cm^3/min) was gradually introduced to the cell reactor with the aid of a water pump fed with double-distilled H_2O and a heater, by simultaneously removing the corresponding amount of Ar flow. After reaching steady state, a 10 v/v% H_2S/Ar mixture (Air Liquide) at the appropriate flow was also fed into the cell reactor to result in reaction mixtures containing 0–1 v/v% H_2S, 90 v/v% H_2O with Ar as a diluent.

Impedance measurements were performed in two-point/four wire configurations. Two wires (current lead and voltage probe) were contacted to the top (working) and the bottom (counter, contacted by the low current lead) electrodes. The impedance measurements were carried out with an oscillating 25 mV RMS voltage in the frequency range from 0.5 MHz to 1 μHz, using a Versa Stat 4 electrochemical workstation by Princeton Applied Research and the relevant software (Versa Studio) for data processing.

A sole symmetrical cell was employed for all measurements. The overall series of experiments (effect of H_2S feed concentration and cell temperature) was carried out as a step change test, where the duration of each step was equal to 3 h and impedance spectra were acquired every 30 min. Initially, the effect of H_2S feed concentration (0–1.0 v/v %) in excess water (90 v/v%) with Ar as diluent was explored, at 850 °C. In the beginning, the cell was exposed for 3 h to a 90 v/v% H_2O/Ar mixture and then the feed was switched to a 0.25 v/v% H_2S, 90 v/v% H_2O diluted in Ar mixture and the impedance behavior of the cell was monitored for 3 h, every 30 min. Following that step, the H_2S feed concentration changed to 0.5 v/v% and the same procedure was repeated. Finally, a mixture of 1.0 v/v% H_2S, 90 v/v% H_2O diluted in Ar was introduced in the cell and impedance measurements were elaborated at different cell temperatures by decreasing the temperature with a step of 50 °C from 850 to 700 °C. Again, the duration of each temperature step was equal to 3 h and impedance measurements were carried out every 30 min.

In all cases, the cell impedance was normalized by the geometric area of the symmetrical cell, thus all resistance values are expressed in this work in Ω·cm^2. The impedance data was deconvoluted by using the *Z*-view software from Scribner Associates and by applying a Randle's type of equivalent circuit as presented in Fig. 2. The circuit was, if necessary, modified with a Gerischer element, accounting for a distributed chemical-electrochemical reaction series giving asymmetric impedance responses, such as drop-shaped semi-circles.

The total mass transfer resistance reported here is always the sum of Rmt + R_G, if the Gerischer element is used in the deconvolution. R_G is then the Gerischer resistance at DC, calculated as $R_G(\omega = 0) = \frac{1}{Y_0\sqrt{k}}$. The "rate constant" parameter, k, expressed in s^{-1}, represents the effective transfer rate of the chemical reaction, while the "admittance" parameter, Y_0 expressed in $S.s^{1/2}$, has the same definition as for the Warburg impedance.

3. Results and discussion

3.1. Electrochemical impedance spectroscopy studies

3.1.1. Effect of H_2S feed concentration

Fig. 3 depicts the open circuit AC impedance spectra of the symmetrical cell, Co_3O_4-CeO_2/BZCY72/Co_3O_4-CeO_2, under different H_2S concentrations (0–1 v/v% H_2S) in the presence of excess H_2O (90 v/v%) conditions, at 850 °C. The corresponding fitting curves, accord-

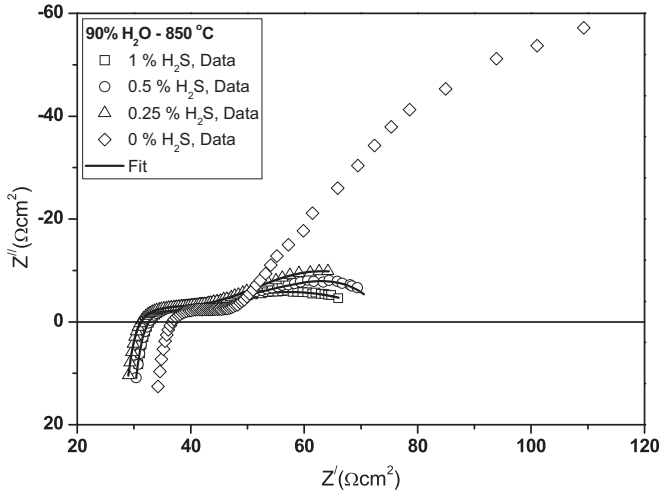

Fig. 3. AC impedance spectra and corresponding fitting curves at different H_2S concentrations. Reaction conditions: 0, 0.25, 0.5 and 1.0 v/v% H_2S, 90 v/v% H_2O diluted in Ar, F_t = 100 cm^3/min, T = 850 °C.

ing to the equivalent circuit model (Fig. 2) are also shown. It should be noted here, that the experiments were carried out as 3 h step change tests, starting from H_2S-free atmospheres (90 v/v% H_2O diluted in Ar) to H_2S-containing feed compositions by increasing stepwise the H_2S concentration from 0.25 to 0.5 and finally 1.0 v/v%. The values for overall cell conductivity and electrode polarization resistance characteristics derived from fitting are listed in Table 1.

It is evident that the overall cell conductance is improved upon addition of 0.25% H_2S, although it is independent of further increased H_2S concentration. In particular, the electrolyte conductivity, σ, increases from 1.5×10^{-3} S·cm^{-1} in the absence of H_2S to ca. 1.8×10^{-3} S·cm^{-1} in H_2S-containing environments. A similar picture is also obtained for the electrode polarization resistance; Rp drastically decreases from 277 Ω·cm^2 in the absence of H_2S to ca. 48 Ω·cm^2 in the presence of 0.25% H_2S in the feed stream, then slightly decreasing by further increasing the H_2S concentration to 0.5 and 1.0 v/v%.

The above findings can be well rationalized on the basis of chemical and electrochemical processes taking place on the symmetrical cell, Co_3O_4-CeO_2/BZCY72/Co_3O_4-CeO_2, when it is exposed to different H_2S-H_2O-Ar containing mixtures. At the gas phase and on the electrodes surface the following stoichiometries are carried out:

$$H_2S + 2H_2O \leftrightarrow 3H_2 + SO_2 \quad (1)$$

$$H_2S \leftrightarrow 1/nS_n + H_2 \quad (2)$$

while at the anode three-phase-boundary (tpb) the produced H_2 from reactions (1) and (2) along with the co-electrolysis of H_2S (4) and H_2O (5) could generate protons (H^+), which are transported to the cathode tpb toward H_2 evolution (6):

Anode half-cell reactions:

$$H_2 \rightarrow 2H^+ + 2e^- \quad (3)$$

$$H_2S \rightarrow 2H^+ + 1/nS_n + 2e^- \quad (4)$$

$$H_2O \rightarrow 2H^+ + 1/2O_2 + 2e^- \quad (5)$$

Cathode half-cell reactions:

$$2H^+ + 2e^- \rightarrow H_2 \quad (6)$$

The pronounced effect of H_2S addition can be, inter alia, assigned to the in situ generated H_2 via the gas phase and surface reactions (1) and (2) and/or to the structural/morphological modifications of the electrode induced by its interaction with the H_2S/H_2O reacting mixture and the associated reaction intermediates. Both parameters can enhance to a different extend the electrode kinetics, while the latter clearly affects the electrode in-plane conductivity by utilizing better more of the electrolyte. However, on the basis of the present results, no definitive conclusions in relation to the precise effect of each parameter on the electrochemical performance can be obtained.

In general, the features of the AC impedance spectra are comprised of two arcs, one centered at high frequencies (HF) and the other one at lower frequencies (LF), with the latter dominating the polarization resistance, as obviously seen for the 90 v/v% H_2O/Ar mixture (Fig. 3). Based on the pseudo-capacitance values, of 10^{-6}–10^{-5} and 10^{-3}–10^{-2} F·cm^{-2} for the HF and LF arcs, respectively, it can be safely assumed that the HF arc is attributed to charge transfer processes, while the LF arc is reflecting mass transfer limitations, associated with the adsorption/diffusion of reactions (1) and (2) intermediates. From the corresponding values in Table 1, it is evident that the adsorption, diffusion and surface reaction steps are the main contributors to the overall electrode polarization resistance.

3.1.2. *Effect of cell temperature*

In the following, the same symmetrical cell was employed to assess the effect of temperature at a constant feed composition. It should be again mentioned that the duration of each temperature step was equal to 3 h and impedance spectra were acquired every 30 min. Fig. 4 presents the open circuit impedance spectra and the corresponding deconvoluted fitting curves of the symmetrical cell at various temperatures ranging from 700 to 850 °C, with a standard feed mixture containing 1 v/v% H_2S, 90 v/v% H_2O, diluted in Ar.

In Table 2, the fitting values for cell conductivity, electrode polarization, charge transfer and mass transfer resistances, are listed. The pronounced effect of temperature is clear, increasing the electrolyte conductivity from 0.7×10^{-3} S·cm^{-1} at 700 °C to 1.7×10^{-3} S·cm^{-1} at 850 °C, with an activation energy, equal to 53.2 kJ/mol. Similar values of conductivity, i.e., 2.03×10^{-3} S·cm^{-1}, were also reported for the Pt/$BaZr_{0.85}Y_{0.15}O_{3-\delta}$/Pt cell at 650 °C, when exposed to 0.5 H_2S/H_2 mixtures [17].

Again, the dominant feature in the impedance spectra (Fig. 4) is comprised of a small high frequency (HF) arc overlapped with a large arc at low frequencies (LF), while the size of both arcs, reflecting the electrode polarization resistance, decreases significantly by increasing the cell temperature. This is also reflected on the calculated values of Rp, Rct and Rmt, which are sufficiently improved as the cell temperature increases, with activation energies equaled to 83.3, 29.7 and 92.0 kJ/mol, respectively (Fig. 5). From the acquired data, it is evident that as the temperature increases, the surface kinetics are faster and the contribution of the charge transfer processes becomes more critical on the overall cell performance, beginning with 20% at 700 °C and reaching almost 40% of the overall electrode polarization at 800 °C. The charge transfer contribution compared to mass transfer processes is

Table 1
Overall cell conductivity and polarization resistance characteristics as a function of feed composition, at T = 850 °C.

Feed mixtures	Overall electrolyte conductivity, σ (S·cm^{-1})	Electrode polarization resistance, Rp (Ω·cm^2)	Charge transfer resistance, Rct (Ω·cm^2)	Mass transfer resistance, Rmt (Ω·cm^2)
90% H_2O/Ar	1.5×10^{-3}	277	16.3	260
0.25% H_2S/90% H_2O/Ar	1.8×10^{-3}	49.7	14.7	35.0
0.50% H_2S/90% H_2O/Ar	1.8×10^{-3}	47.7	15.7	32.0
1.00% H_2S/90% H_2O/Ar	1.7×10^{-3}	47.5	14.1	33.4

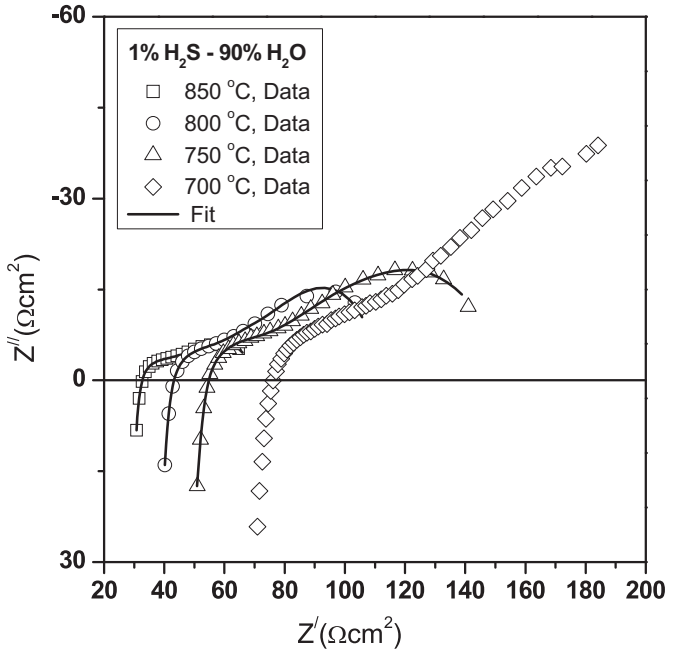

Fig. 4. Impedance spectra and corresponding fitting curves as a function of cell temperature (700–850 °C). Reaction conditions: 1 v/v% H_2S, 90 v/v% H_2O diluted in Ar, F_t = 100 cm^3/min.

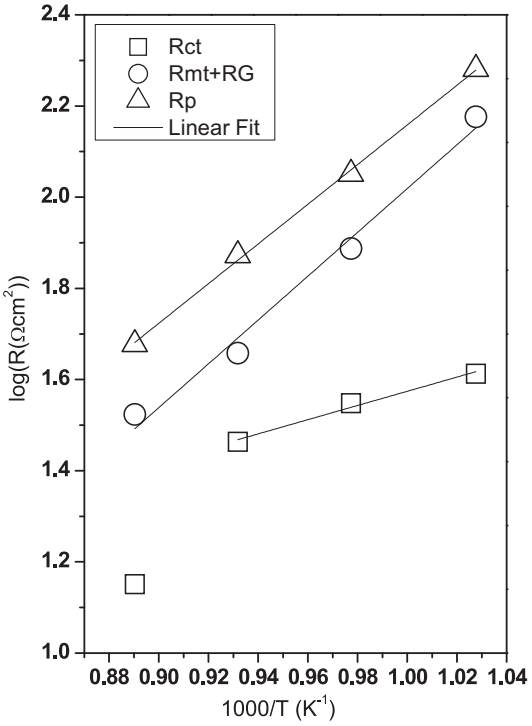

Fig. 5. Arrhenius plots of electrode polarization, Rp, charge transfer, Rct, and mass transfer, Rmt, resistances. Reaction conditions: 1 v/v% H_2S, 90 v/v% H_2O diluted in Ar, F_T = 100 cm^3/min.

Table 2
Overall electrolyte conductivity and polarization resistance characteristics as a function of temperature at a constant feed composition of 1 v/v% H_2S, 90 v/v% H_2O diluted in Ar.

Temperature (°C)	Overall electrolyte conductivity, σ ($S{\cdot}cm^{-1}$)	Electrode polarization resistance, Rp ($\Omega{\cdot}cm^2$)	Charge transfer resistance, Rct ($\Omega{\cdot}cm^2$)	Mass transfer resistance, Rmt ($\Omega{\cdot}cm^2$)
700	0.7×10^{-3}	191	41.0	150
750	1.0×10^{-3}	112	35.3	77.2
800	1.3×10^{-3}	74.5	29.1	45.4
850	1.7×10^{-3}	47.5	14.1	33.4

lowered at 850 °C, which could be attributed to the red-ox processes of intermediate reaction products (e.g., sulfur-containing species) or to the partial O^{2-} transport of BZCY72 at high temperatures, as it has been observed in previous relevant works [18,19]. For this reason, the activation energy for Rct (29.7 kJ/mol) has been calculated taking into account the corresponding values in the temperature range of 700–800 °C, thus excluding the point at 850 °C.

3.2. Physicochemical characterization studies

To gain insight into the impact of reaction atmosphere on the structural/morphological features of cell constituents, and their consequent effect on the above described electrochemical performance, a SEM/EDS and XRD analysis of samples before and after measurements was carried out. Fig. 6 shows SEM pictures of the fresh Co_3O_4/CeO_2 electrode surface (Fig. 6A), as well as of the cross section image of the corresponding Co_3O_4-CeO_2/BZCY72 interface (Fig. 6B). Two distinct phases, i.e., cobalt oxide (darker features) and ceria (brighter features) were identified in the fresh sintered electrode, with a grain size of 1–5 μm. In the cross section (Fig. 6B), a two layer structure, consisting of a dense electrolyte and a porous electrode with thickness of 20 μm, is observed. The BZCY72 retained its dense and crack-free microstructure after electrode calcination, demonstrating that blade-aided electrode printing at 1400 °C is a suitable method for the fabrication of Co_3O_4/CeO_2 supported cells, based on BZCY72 electrolytes. Moreover, it should be noticed that although a high sintering temperature was selected to obtain a good Co_3O_4/CeO_2 electrode layer adhesion on the BZCY72 surface, no chemical reactions at the electrode/electrolyte interface were observed, by the SEM and EDS studies.

The XRD spectrum (not shown) of the fresh sample revealed only reflections corresponding to Co_3O_4, CeO_2, and BZCY72, verifying that no chemical transformations or interactions between the two oxides and the electrolyte occurred up to 1400 °C in air. However, in the case of the aged sample, the CoO phase was additionally identified, indicating the reduction of cobalt oxide by the in situ produced H_2 from reactions (1) and (2). On the other hand, no change in BZCY72 structure was observed, verifying its chemical stability in H_2S-containing atmospheres [20].

Corresponding SEM micrographs of the used electrode surface and cell cross section are shown in Fig. 7. By comparing the SEM pictures of the fresh (Fig. 6A) and used (Fig. 7A) samples, it is evident that the electrode has undergone significant morphological modifications, leading to new phases and a better porosity, as a result of its exposure in H_2S-containing environments at high temperatures. In particular, the average size of the cobalt containing particles increased to 10 μm, forming a worm-like shape, overlapping the smaller CeO_2 particles which are located at the bottom edges of the cobalt species. Moreover, EDS analysis of the cobalt containing agglomerates revealed the existence of cobalt sulfides. In view of this fact, the superiority of Co_3O_4/CeO_2 catalysts toward H_2S decomposition to H_2 in both dry and wet (90% v/v) atmospheres can be attributed to the in situ sulfidation of catalysts active counterparts (Co_3O_4 to $Co_{1-X}S_Y$ and CeO_2 to $Ce_{10}S_{14}O_Y$) during the exposure under reaction conditions [15]. On the contrary, the BZCY72 pellet remained dense and stable (Fig. 7B), demonstrating its tolerance to H_2S presence, a behavior also observed in [17] and for $BaCe_{0.8-X}Zr_XY_{0.2}O_{3-\delta}$ (with $0.4 \leq \times \leq 0.8$) after treatment with 10 v/v% H_2S/Ar at 700 °C for 10 h [21].

At this point it may be noticed that only few studies have addressed the effect of H_2S on the electrochemical performance of proton conducting ceramic cells, whereas most of these are mainly focused on the chemical stability of the solid electrolyte rather than the

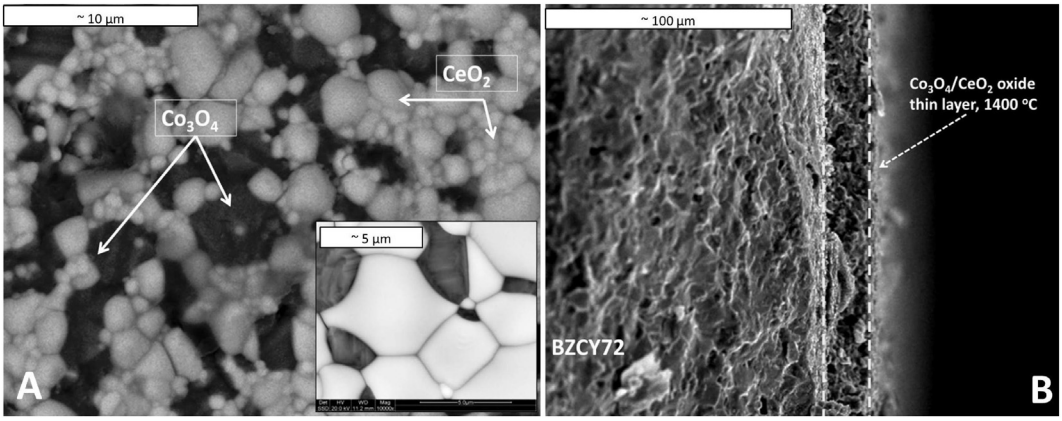

Fig. 6. A) SEM pictures of the fresh calcined Co_3O_4/CeO_2 electrode surface at two different magnifications. B) Cross section image of the fresh Co_3O_4-CeO_2/BZCY72 interface.

electrode [17,21,22].

In light of the above, the present work was focused on the electrochemical performance and stability of Co_3O_4/CeO_2 electrodes exposed to H_2S/H_2O atmospheres, by employing a proton conducting symmetrical cell, with BZCY72 as the solid electrolyte. AC impedance measurements at different H_2S feed concentrations and temperatures employing step change stability tests coupled with XRD and SEM studies of fresh and used electrodes, were employed to assess the electrochemical performance of Co_3O_4/CeO_2 composites. It was found that upon increasing temperature and H_2S concentration, the overall cell conductivity, electrode resistance and as a consequence the electrochemical performance, although not sufficiently high for practical applications, is substantially improved, being remarkably stable even after the step change experiments at H_2S-containing environments (of 21 h total duration).

The AC impedance spectra indicated two contributions attributed to the charge transfer and mass transport processes, with the latter being associated with the chemical steps (adsorption, diffusion, surface reaction) of reactions (1) and (2) intermediates. Moreover, the SEM and XRD studies of the aged electrodes showed that the Co_3O_4/CeO_2 electrode undergoes significant structural/morphological alterations, due to its exposure to $H_2S/H_2O/Ar$ feed mixtures. In specific, part of the initial Co_3O_4 is reduced to CoO by the in situ produced hydrogen, while both electrode counterparts (CeO_2 and Co_3O_4) have grown in size and transformed to sulfides by the interaction with the reactions (1) and (2) intermediates, simultaneously rearranged on the electrode surface. These modifications may be responsible for the improved electrochemical performance, since they can lead to i) more active electrode surfaces, ii) better distributed cobalt-rich particles enhancing the electrode in-plane conductivity and thus its electronic percolation and iii) better porosity, facilitating the mass transfer processes.

4. Conclusions

The electrochemical behavior of Co_3O_4/CeO_2 composite in H_2S-containing atmospheres under excess H_2O (90 v/v%) conditions was examined in a proton conducting ceramic symmetrical cell of the type Co_3O_4-CeO_2/BZCY72/Co_3O_4-CeO_2. AC impedance spectroscopy studies, at different H_2S feed concentrations (0–1 v/v%) and temperatures (700–850 °C), in conjunction with physicochemical characterization measurements of the fresh and aged (after H_2S-treatment) electrodes/cells, were employed to systematically assess the electrochemical performance and stability behavior of the electrode. A promising stable electrochemical behavior was achieved, being favored as the H_2S feed composition and cell temperature increased. AC impedance spectra revealed contributions from charge transfer and mass transport steps, with the latter being in general more critical for the overall system, associated with the adsorption, diffusion and surface processes of the $H_2S + 2\ H_2O \leftrightarrow 3\ H_2 + SO_2$ and H_2S decomposition reactions intermediates. Although the electrolyte (BZCY72) itself was not affected by the H_2S treatment, significant modifications in the structural phases and morphology of the electrode were observed by the SEM and XRD studies of the used samples. The in situ reduction and sulfidation of the electrode results in more active surfaces with higher porosity and better

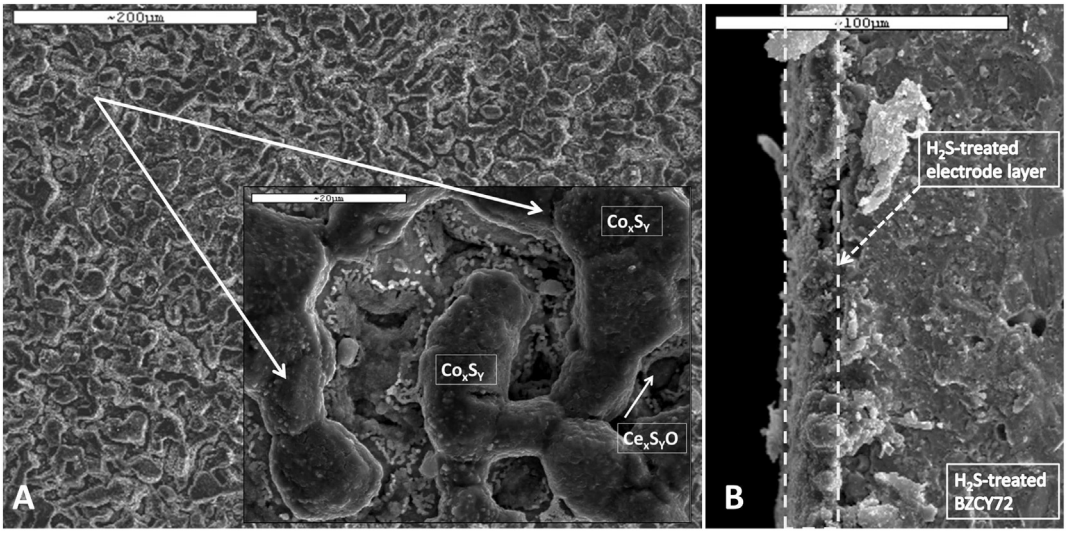

Fig. 7. A) SEM pictures of the aged Co_3O_4/CeO_2 electrode at two different magnifications. B) Cross section image of the aged Co_3O_4-CeO_2/BZCY72 interfase.

electronic conductivity, facilitating both the charge transfer and mass transport processes. The stable electrochemical performance of Co_3O_4/CeO_2 composites under H_2S-H_2O atmospheres may open new perspectives for the development of efficient, IRES powered, proton conducting ceramic H_2S and H_2O co-electrolysis cells toward "green" hydrogen production. Work in this direction is currently in progress.

Acknowledgements

Part of this work was realized via the program "Scholarships of IKY in the Marine and Inland Management of Water Resources" (Contract Nr. 11) and was co-funded by EEA grants– Financial Mechanism 2009–2014 (85%) and the General Secretariat for Investments and Development (15%).

References

[1] M. Midilli, A. Aya, N. Kale, Veziroglu, A parametric investigation of hydrogen energy potential based on H_2S in Black Sea deep waters, Int. J. Hydrog. Energy 32 (2007) 117–124.
[2] Paris Agreement, United Nations Framework Convention on Climate Change. http://unfccc.int/files/essential_background/convention/application/pdf/english_paris_agreement.pdf, (2015) accessed 10.12.16.
[3] K. Fukuda, M. Dokiya, T. Kameyama, Y. Kotera, Catalytic decomposition of hydrogen sulfide, Ind. Eng. Chem. Fundam. 17 (1978) 243–247.
[4] D. Ipsakis, Tz. Kraia, G.E. Marnellos, M. Ouzounidou, S. Voutetakis, R. Dittmeyer, A. Dubbe, K. Haas-Santo, M. Konsolakis, H.E. Figen, N.O. Güldal, S.Z. Baykara, An electrocatalytic membrane-assisted process for hydrogen production from H2S in Black Sea: preliminary results, Int. J. Hydrog. Energy 40 (2015) 7530–7538.
[5] E. Luinstra, H_2S: a potential source for hydrogen, Sulphur 244 (1996) 37–47.
[6] J. Zaman, A. Chakma, Production of hydrogen and sulphur from hydrogen sulphides, Fuel Process Technol. 41 (1995) 159–198.
[7] J. Li, J.L. Luo, K.T. Chuang, A.R. Sanger, Proton conductivity and chemical stability of Li_2SO_4 based electrolyte in a H_2S-air fuel cell, J. Power Sources 160 (2006) 909–914.
[8] S.V. Slavov, K.T. Chuang, A.R. Sanger, J.C. Donini, J. Kot, S. Petrovic, A proton-conducting solid state H_2S-O_2 fuel cell. 1. Anode catalysts, and operation at atmospheric pressure and 20–90 °C, Int. J. Hydrog. Energy 23 (1998) 1203–1212.
[9] E. Fabbri, D. Pergolesi, E. Traversa, Materials challenges toward proton-conducting oxide fuel cells: a critical review, Chem. Soc. Rev. 39 (2010) 339–359.
[10] L. Malavasi, C.A.J. Fisher, M.S. Islam, Oxide-ion and proton conducting electrolyte materials for clean energy applications. Structural and mechanistic features, Chem. Soc. Rev. 39 (2010) 4370–4387.
[11] V. Vorontsov, J.L. Luo, A.R. Sanger, K.T. Chuang, Synthesis and characterization of new ternary transition metal sulphide anodes for H_2S-powered solid oxide fuel cell, J. Power Sources 183 (2008) 76–83.
[12] M. Gong, X. Liu, J. Trembly, C. Johnson, Sulfur-tolerant anode materials for solid oxide fuel cell application, J. Power Sources 168 (2007) 289–298.
[13] M. Konsolakis, The role of copper–ceria interactions in catalysis science: recent theoretical and experimental advances, Appl. Catal. B Environ. 198 (2016) 49–66.
[14] A. Atkinson, S. Barnett, R.J. Gorte, J.T.S. Irvine, A.J. McEvoy, M. Mogensen, S.C. Singhal, J. Vohs, Advanced anodes for high-temperature fuel cells, Nat. Mater. 3 (2004) 17–27.
[15] Tz. Kraia, M. Konsolakis, G.E. Marnellos, H_2S in Black Sea: turning an environmental threat to an opportunity for clean H_2 production via an electrochemical membrane reactor, Research Progress in H_2S-PROTON Project, MATEC Web Conf. 41, 2016 (04002).
[16] NorECs, Norwegian Electro Ceramics AS. http://www.norecs.com http://www.norecs.com/index.php?page=Newsletter+154 (accessed 08.12.16).
[17] J. Li, J.-L. Luo, K.T. Chuang, A.R. Sanger, Chemical stability of Y-doped $Ba(Ce,Zr)O_3$ perovskites in H_2S-containing H_2, Electrochim. Acta 53 (2008) 3701–3707.
[18] R. Strandbakke, O. Dyrlie, F.S. Hage, T. Norby, Reaction kinetics of protons and oxide ions in LSM/lanthanum tungstate cathodes with Pt nanoparticle activation, J. Electrochem. Soc. 163 (2016) 507–515.
[19] R. Strandbakke, V.A. Cherepanov, A.Y. Zuev, D.S. Tsvetkov, C. Argirusis, G. Sourkouni, S. Prünte, T. Norby, Gd- and Pr-based double perovskite cobaltites as oxygen electrodes for proton ceramic fuel cells and electrolyser cells, Solid State Ionics 278 (2015) 120–132.
[20] J.M. Polfus, T. Norby, R. Bredesen, Protons in oxysulfides, oxysulfates, and sulfides: a first-principles study of La_2O_2S, $La_2O_2SO_4$, $SrZrS_3$, and $BaZrS_3$, J. Phys. Chem. C 119 (2015) 23875–23882.
[21] D. Medvedev, J. Lyagaeva, S. Plaskin, A. Demin, P. Tsiakaras, Sulfur and carbon tolearance pf $BaCeO_3$-$BaZrO_3$ proton conducting materilas, J. Power Sources 273 (2015) 716–723.
[22] M. Gong, X. Liu, J. Trembly, C. Johnson, Sulfur-tolerant anode materials for solid oxide fuel cell application, J. Power Sources 168 (2007) 289–298.